Catalysis Letters, Vol. 116, Nos. 1–2, July 2007 (© 2007)
DOI: 10.1007/s10562-007-9121-x

Adsorption of iso-/*n*-butane on an anatase thin film: a molecular beam scattering and TDS study

J. Goering,[a] E. Kadossov,[a] U. Burghaus,[a,*] Z. Q. Yu,[b,c] S. Thevuthasan,[b] and L. V. Saraf[b]

[a]*Department of Chemistry, North Dakota State University, Fargo, ND , USA*
[b]*Pacific Northwest National Laboratory, Richland, WA , USA*
[c]*Department of Chemistry, Nanjing Normal University, Nanjing, China*

Received 3 April 2007; accepted 3 April 2007

Binding energies and adsorption probabilities have been determined for *n*/iso-butane adsorption on an anatase thin film grown on $SrTiO_3$(001) by means of thermal desorption spectroscopy (TDS) and molecular beam scattering. The sample has been characterized by X-ray diffraction (XRD) and Auger electrons spectroscopy (AES).

KEY WORDS: gas surface interactions; adsorption dynamics; molecular beam scattering; adsorption kinetics; thermal desorption spectroscopy; alkanes; anatase thin film.

1. Introduction

Titanium dioxide has a wide range of technical applications, it is used for the design of sensors [1], solar cells [2], and batteries [3] as well as a part of catalysts for a variety of surface reactions including CO oxidation [4], selective catalytic reduction [5] of NO_x, and water decomposition [6]. Although TiO_2 exists in different crystallographic phases, most surface science studies have focused on rutile TiO_2(110). However, industrial TiO_2 powder catalysts consist of rutile and anatase crystallites. Moreover, it has been proposed [7, 8] that the most catalytically active polymorph is anatase. Anatase films grown on single crystal supports [9] (as used here) allow to apply ultra-high vacuum surface chemistry techniques to characterize its catalytic activity. Information about what crystallographic orientation dominates TiO_2 powder catalysts is quite diverse. According to a transmission electron microscopy study [10], TiO_2 P25 and TiO_2 Merck powder catalysts are dominated by (001) and (010) anatase surface planes. In addition, it has been proposed that anatase (001) is the active phase for photocatalytic water decomposition [11, 12]. Therefore, studies on anatase thin films grown on $SrTiO_3$(001) appear pertinent. Another motivation concerns TiO_2 nanotubes and nanoparticles which are, due to its smaller surface energy [13], formed from the anatase polymorph (Hokkanen *et al.*, in preparation) [14, 15]. Therefore, anatase thin films also can be considered the planar counterpart of TiO_2 based nanomaterials [16].

*To whom correspondence should be addressed.
E-mail: uwe.burghaus@ndsu.edu

The chemical properties of hydrocarbons have been studied extensively in surface science and catalysis due to their importance for the petroleum industry and sustainable energy research. Therefore, kinetic parameters of alkane adsorption/desorption have been obtained by thermal desorption spectroscopy (TDS) for a large variety of single crystal surfaces including graphite [17], sapphire [18], ZnO [19], Pt [20], Ru [21], Cu [22, 23], and C-/TiO_2 nanotubes [15]. Furthermore, molecular beam scattering techniques have been applied to characterize the adsorption dynamics (i.e. gas-surface energy transfer processes) [24] and numerous theoretical studies [25] have been conducted. Alkanes commonly adsorb molecularly with lateral interactions causing TDS peak shifts. At low adsorption temperatures, condensation in bi- and multilayers leads to additional TDS features. At low surface temperatures precursor mediated adsorption typically dominates the adsorption dynamics, i.e. coverage dependent adsorption probabilities, $S(\Theta)$, are approximately independent of coverage, consistent with Kisliuk's precursor model. In the limit of large impact energies of the alkane an initial increase in $S(\Theta)$ with Θ is often observed, which can be explained qualitatively by mass-matching considerations [26,27].

2. Materials and experimental procedures

At Pacific Northwest National Laboratories an anatase TiO_2(001) film has been grown on a $SrTiO_3$(001) support employing an oxygen plasma-assisted molecular beam epitaxy (MBE) system [9]. The sample has been characterized by X-ray diffraction (XRD) and Auger electron spectroscopy (AES). The TDS and molecular beam scattering measurements have been conducted at

North Dakota State University with a home-built system [28]. The impact energy, E_i, of *n*/iso-butane could be varied within 0.31–1.55 eV by using pure and seeded beams combined with a variation of the nozzle (gas) temperature. The measuring error in the initial adsorption probabilities, S_0, amounts to ± 0.02. The coverage dependent adsorption probability curves, S(Θ), have been smoothed while conserving the shape of the transients. Measurements have been taken for normal impact angles. An exponential background was removed from each TDS curve. The reading of the thermocouple has been calibrated (± 5 K) *in situ* by TDS using the known heat of condensation of the alkanes. A heating rate of 1 K/sec has been used for all TDS measurements. He gas was fluxed through the liquid nitrogen to reduce further the sample temperature.

3. Data presentation and discussion

3.1. Sample characterization

The morphology and cleanliness of the sample has been characterized by XRD and AES as summarized in Figure 1.

XRD scans (Figure 1-I) consist of a superposition of support and anatase peaks, indicating that indeed an anatase thin film was formed in the MBE process due to a better lattice match between anatase and the support versus rutile and $SrTiO_3$(001). The thickness of the film was determined to be 123 nm using X-ray reflectivity (XRR) measurements. AES spectra of the as-prepared sample (transferred through air from the MBE system to the beam scattering apparatus) were dominated by carbon containing impurities with C AES peak intensities roughly twice as large as the Ti AES peak intensity (see curve a in Figure 1-II). Charging of the sample leads to a shift of ~15 eV to larger electron energies as compared with reference data. After mild sputtering (500 eV, 1 μA sample current, 5 min) and annealing cycles (700 K, 1×10^{-6} mbar O_2, 10–20 min) the carbon-to-Ti AES line intensity ratio dropped down to 10% while the Ti-to-O AES peak intensities did not change (see curve b in Figure 1-II). This conventional preparation procedure should heal defects induced by sputtering the surface as well established from studies on metal or metal oxide single crystals. However, it appears plausible that the density of defects of the anatase thin film sample is larger than one typically obtained for metal surfaces or graphite. The strongest support related AES peak position would correspond to Sr excitations at 1640 eV. As shown in the inset of Figure 1-II, no AES lines within the electron energy range of 1500–1800 eV were detected revealing an intact anatase thin film sample. AES spectra have been collected routinely throughout the entire project. The C impurity level did not change for the *n*-/iso-butane experiments.

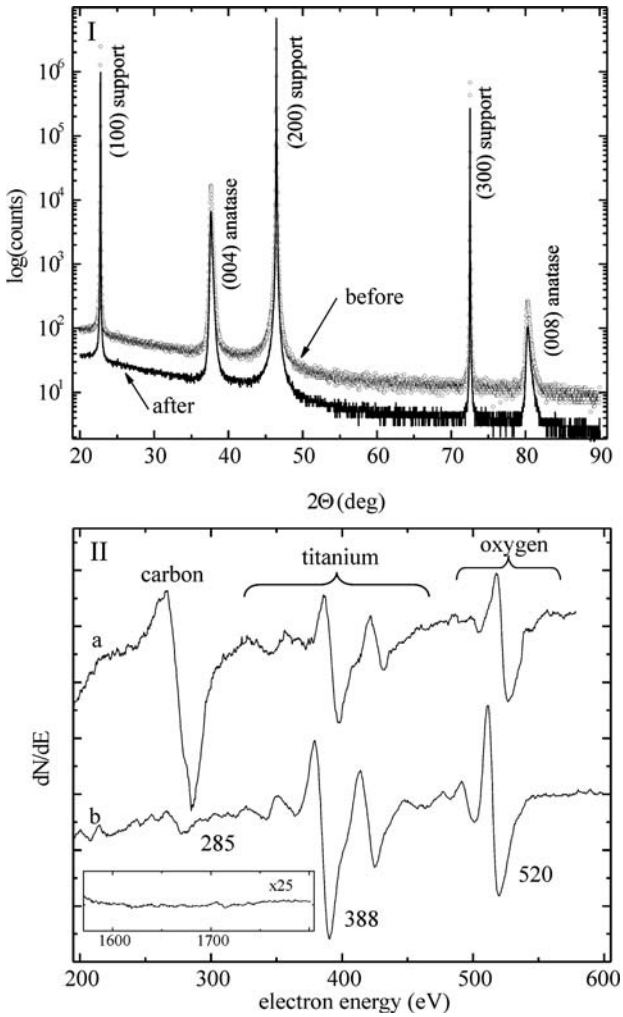

Figure 1. (I) X-ray diffraction (XRD) of the anatase film obtained before and after the kinetics experiments. (II) Auger electron spectra (AES) of (a) the as-prepared anatase thin film sample. (b) After mild sputter-annealing cycles. (AES parameters $E_0 = 2$ keV, $V_{pp} = 10$ V).

3.2. Adsorption kinetics

TDS curves of *n*-butane and iso-butane adsorption as a function of exposure (see Figure caption) at 85–90 K are shown in Figure 2; Figure 3 summarizes the kinetic parameters gathered.

For *n*-butane (Figure 2-I) and at small exposures (see the inset) a single peak (α peak) has been observed, which shifts to lower desorption temperatures with increasing exposure. This, peak shift is consistent either with repulsive lateral interactions of the adsorbates or with the adsorption on different binding sites such as defect and pristine sites. Accordingly, the α peak is assigned to alkane adsorption in the monolayer range. Furthermore, no increase in the C AES peak intensity has been observed after *n*-/iso-butane adsorption/desorption cycles. Thus, bond activation can be ruled out and molecular adsorption is concluded. With increasing exposure a peak grows at 114 K (β peak) and at the largest exposures a structure at 105 K (γ peak)

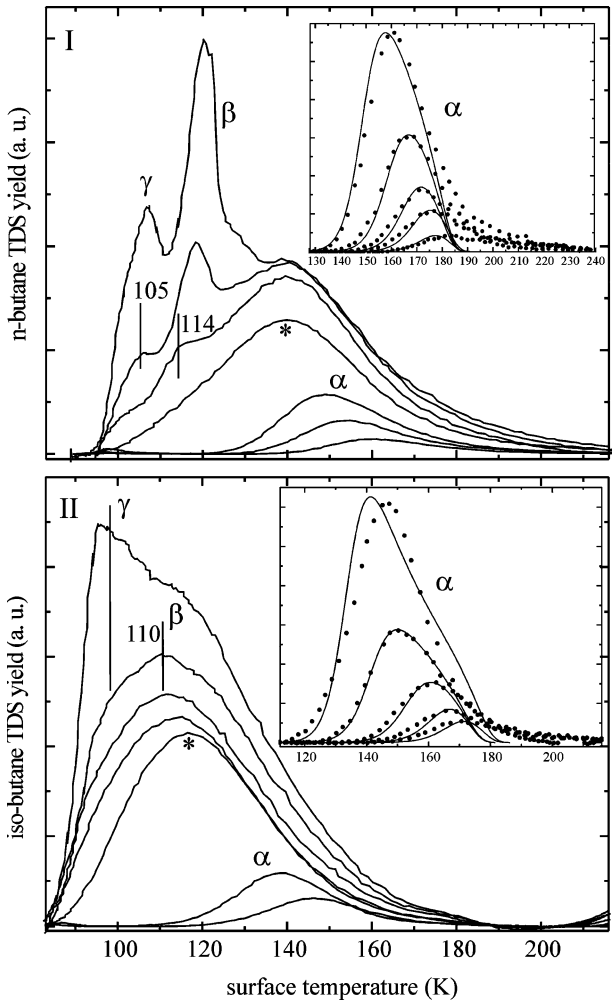

Figure 2. Typical examples of thermal desorption spectroscopy curves for (a) *n*-butane and (b) iso-butane adsorbed on the anatase thin film as a function of exposure. Monolayer, α, bilayer, β, and multilayer, γ, peaks are evident. [Exposures (I) 1, 2, 4, 16, 30 L, inset 0.05, 0.1, 0.2, 0.3, 0.5,1 L. (II) 2, 4, 8, 16, 30, 50, 100 L, inset 0.1, 0.2, 0.3, 0.4, 0.5, 1,2 L]. The solid lines in the inset are the result of fitting the TDS curves by integrating the Polanyi–Wigner equation (see text). (Heating rate = 1 K/sec).

was detected. The leading edges of those low temperature features appear to line up and the β/γ peak positions shift slightly to larger desorption temperatures with increasing coverage. Therefore, these structures are identified as the result of desorption from a bilayer (β) and multilayers (γ).

Similar TDS structures are observed for iso-butane (Figure 2-II). However, the bilayer peak appears at smaller temperatures (110 K) and the adsorption temperature was not low enough to form efficiently multilayers, i.e. only the onset of the γ structure is visible.

The condensation temperature for *n*/iso-butane has been measured before at ultra-high vacuum conditions and was reported as 105.6/101.7 K [29] in agreement with the assignment of the γ peak for *n*-butane as the condensation structure (Figure 2-I). Iso-butane bilayer desorption was observed at 110 K [26] in agreement with the β-peak position shown in Figure 2-II. The shift of 4 K of the condensation temperatures for the two alkanes (as determined before) suggests a similar shift of the bilayer desorption temperatures and hence a bilayer desorption temperature of 114 K for *n*-butane, as indeed observed in our study (Figure 2-I).

In order to obtain coverage dependent binding energies, the TDS curves have been integrated assigning coverage of one monolayer to the TDS curve detected just below the onset of bilayer formation (labeled by an asterix in Figure 2). By means of the Redhead equation the TDS peak positions have been converted into binding energies, E_d, which are shown for an assumed pre-exponential of $\nu = 1 \times 10^{13}$/s as symbols in Figure 3. Accordingly, E_d of both alkanes agrees within the experimental uncertainties. The initial (< 0.1 ML) decrease in E_d is assigned to saturating surface defects by the alkanes, as commonly observed [26, 30]. The slight decrease in E_d at larger coverage ($\Theta > 0.1$ ML) would be consistent with repulsive lateral interactions in agreement with the TDS peak shifts and literature data obtained on other surfaces [18, 26, 31]. The E_d versus Θ curve, as obtained by the Redhead equation, has been parameterized (see the thin solid line and the parameters in the figure caption) and used to generate starting values for a χ^2-fit of the TDS curves by integrating the Polanyi–Wigner equation. The thick solid line in Figure 3 is the result of this fit with the pre-exponential as a variation parameter [30]; the simulated TDS curves are depicted in the inset of Figure 2. This fitting procedure is a compromise leading to reasonable fits of a whole set of *n*/iso-butane TDS curves which allows for a

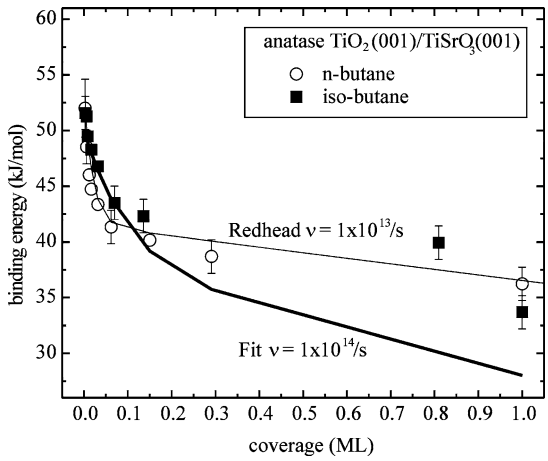

Figure 3. Heat of adsorption, E_d (in kJ/mol), as a function of coverage (symbols) as obtained from the TDS peak positions by means of the Redhead equation and by assuming a standard preexponential of $\nu = 1 \times 10^{13}$/s. The thin solid line is the result of a parameterization by $E_d = 41.5 - 5.0\Theta + 12\exp(\Theta/0.02)$. The thick solid line is based on a direct fit procedure [26, 30] with ν as a variation parameter; $E_d = 38.0 - 10.0\Theta + 12\exp(\Theta/0.10)$ and $\nu = 1 \times 10^{14}$/s have been obtained.

better determination of the pre-exponential factor. Accordingly, a pre-exponential factor larger than the traditionally assumed value leads indeed to a better agreement with the TDS curve shapes which should reproduce the effect of lateral interactions more accurately. However, the Redhead parameterization reproduces naturally the TDS peak positions perfectly.

It is worthy to note that we attempted to collect kinetics data also for longer chain alkanes such as *n*-nonane. However, a large increase in the C AES peak intensity was observed after adsorption/desorption cycles consistent with a bond activation of *n*-nonane [32, 33]. The carbon could only be removed by sputter/annealing cycles which makes it experimentally very difficult to collect kinetics data characterizing competing adsorption pathways (adsorption, decomposition).

3.3. Dynamics

Figure 4 summarizes the molecular beam scattering results. Figure 4-I shows the initial adsorption probabilities, S_0, of iso-/*n*-butane as a function of E_i, and at an adsorption temperature just above the onset of bilayer formation. As an example, the integrated adsorption transients, i.e. the coverage dependent adsorption probabilities, S(Θ), are shown as a function of E_i for iso-butane in Figure 4-II.

3.3.1. Initial adsorption probabilities and the effect of internal molecular excitations

Although no significant difference in the binding energies of the linear and branched alkanes has been observed (Figure 3), interestingly, differences in the adsorption dynamics are evident. S_0 is systematically larger for *n*-butane as compared with iso-butane (Figure 4-I) which appears plausible in regard of their molecular structure. A more spherical molecule such as iso-butane will bounce back from the surface more efficiently than a linear molecule, i.e. the iso-butane surface interaction should be more (quasi)-elastic than the one of *n*-butane. Thus, the energy transfer of the spherical molecule to the surface will be less efficient. Therefore, smaller adsorption probabilities are expected for iso-butane as compared with *n*-butane. The results appear to support this simple rigid molecule model. Note that the same effect has been observed for SiO_2/Si(111) (Funk and Burghaus, in preparation), however, not as distinctly as for the anatase surface. This suggests that the support (and differences in the density of defects) certainly also affects the energy transfer processes.

A different model approach would take the effect of internal degrees of freedom on the adsorption dynamics into account which can depend on the geometry of the molecule [34]. Effects of internal excitations on adsorption probabilities have been reported in a few experimental studies [35, 36]. For physisorption systems, a

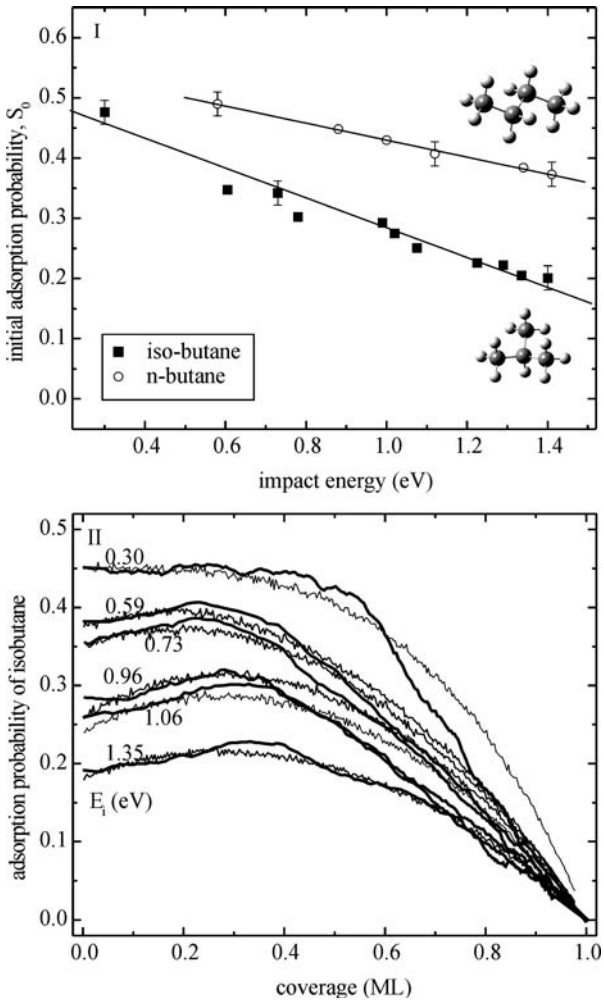

Figure 4. (I) Initial adsorption probability as a function of impact energy for *n*-/iso-butane obtained just above the condensation temperatures (adsorption temperature of 135/115 K). For a given impact energy, the gas temperatures are approx. identically for *n*- and iso-butane. (The linear fit is shown as a guide for the eye with the following parameters for iso-butane $S_0 = -0.23\ \{E_i + 0.51$ and *n*-butane $S_0 = -0.15\ E_i + 0.58$ with E_i in eV). (II) Coverage dependent adsorption probability (thick lines) at 115 K for iso-butane and parametric in impact energy. (S_0 has been normalized according to the solid line fit shown in panel I) The thin lines are the result of a Monte Carlo simulation [37].

suppression of the adsorption by rotational energy has been observed [35]. This can be understood as sterically hindered adsorption. Rotations can decrease the gas-surface interaction time for molecule with the right orientation with respect to the surface. Although at the same gas temperature (Figure 4-I) energetically higher rotational modes will be excited for a spherical molecule, we may speculate that the rotational energy should affect the adsorption of a linear molecule more strongly than for a spherical molecule. However, despite a possible suppression of the adsorption by internal molecular rotations expected to be most distinct for the linear molecule, S_0 of *n*-butane is larger than for iso-butane. In addition, the vibrational degrees of freedom should

influence the adsorption similarly for linear and spherical molecules. Therefore, it appears unlikely that differences in the internal excitations of the molecules are the main reason for the differences seen in S_0. The rigid molecule model provides currently the most plausible explanation. However, further studies will be required to definitely identify the influence of internal excitations of alkanes on the adsorption dynamics for anatase thin films.

The overall decrease in S_0 with increasing E_i simply reflects a decreasing efficiency in gas-surface energy transfer processes at larger impact energies. Furthermore, S_0 decreasing with E_i is consistent with non-activated precursor mediated adsorption.

3.3.2. Coverage dependent adsorption probabilities

The S(Θ) curves (Figure 4-II) are at low impact energies ($E_i < 0.3$ eV) consistent with the traditional Kisliuk model. Thus, the adsorption dynamics is precursor mediated. At large ($E_i > 0.3$ eV) impact energies, S(Θ) initially increases, a commonly observed effect [27] called adsorbate-assisted adsorption. The simplest explanation assumes an enhancement in gas-surface energy transfer processes with increasing coverage due to an increase in the overall (gas-surface) mass-match with increasing Θ. Adsorbate-assisted adsorption is typically observed at large impact energies and low adsorption temperatures (i.e. at large surface coverage), as it is also the case for the anatase system studied here.

To obtain additional information, Monte Carlo simulations (MCS) of the S(Θ) curves have been conducted. The algorithm [37] includes two parameters, the trapping probability in the extrinsic precursor state and a lifetime parameter (number of hops); tests of this MCS scheme are given in refs [27, 38]. The experimental curves could be reasonably well reproduced. The trapping probability decreases from 0.55 to 0.42 with increasing impact energy (0.3–1.35 eV) following the observed trend in S_0.

4. Summary and conclusions

The following information has been collected for an anatase thin film sample:

- Iso-/*n*-butane adsorption is molecular and non-activated as concluded from TDS and beam scattering data.
- Besides monolayer TDS peaks, bilayer and multilayer TDS structures have been observed in agreement with prior studies.
- The coverage dependent binding energies, $E_d(\Theta)$, of *n*/iso-butane agree within the experimental uncertainties.
- TDS peak positions shift to lower temperatures with increasing coverage of the alkanes which is consistent either with the effect of lateral interactions of the adsorbates or the population of different adsorption sites.
- $E_d(\Theta)$ has been determined by the Redhead equation as well as by directly fitting the TDS curves leading to a better estimate of the pre-exponential factor.
- It appears that longer chain alkanes such as n-nonane dissociate already below 300 K and at thermal impact energies (backfilling experiments).
- The adsorption dynamics is precursor-mediated obeying the Kisliuk precursor model at low impact energies and the adsorbate-assisted adsorption effect at large impact energies.
- Trapping probability in the precursor state have been obtained by Monte Carlo simulations.
- Although no significant differences in the adsorption kinetics was present for iso-/*n*-butane, the adsorption dynamics depend distinctly on the molecular structure of the alkane.
- Interestingly, the gas-surface energy transfer processes are more efficient for the linear alkane as compared with the branched alkane which leads to systematically smaller S_0 values for the latter molecule qualitatively consistent with a simple rigid molecule model.
- Demonstrated is the feasibility of conducting experiments on a well defined anatase thin film sample transferred through air from one location to another laboratory.

Acknowledgments

Financial support by the DoE-EPSCoR (DE-FG02-06ER46292, state grant) and from ND NSF-EPSCoR IIP seed (EPS-047679) is acknowledged. Work was also performed in the Environmental Molecular Sciences Laboratory, a national scientific user facility sponsored by the Department of Energy (DoE).

References

[1] W. Goepel, J. Hesse and J.N. Zeinel, *Sensors a comprehensive survey* (VCH, Weiheim, 1991).
[2] B.O. Regan and M. Graetzel, Nature 353 (1991) 737.
[3] S.Y. Huang, L. Kavan, I. Exnar and M. Graetzel, J. Electrochem. Soc. 142 (1995) L142.
[4] M. Haruta, Catal. Today 36 (1997) 153.
[5] V.I. Parvulescu, P. Grange and B. Delmon, Catal. Today 46 (1998) 233.
[6] L. Kavan, M. Gratzel, S.E. Gilbert, C. Klemenz and H.J. Scheel, J. Am. Chem. Soc. 118 (1996) 6716.
[7] C.N. Satterfiled, *Heterogeneous Catalysis in Industrial Practice* (McGraw-Hill, Inc., New York, 1991).
[8] T.L. Thompson and J.T. Yates, Chem. Rev. 106 (2006) 4428.
[9] A. Chambers, C.W. Wang, S. Thevuthasan, I. Droubay, D.E. Mccready, A.S. Lea, V. Shutthanandan and C.F. Windisch, Thin Solid Films 418 (2002) 197.
[10] G. Martra, Appl. Catal. A Gen. 200 (2000) 275.

[11] A. Fujishima and K. Honda, Nature 238 (1972) 37.
[12] G.S. Herman, M.R. Sievers and Y. Gao, Phys. Rev. Lett. 84 (2000) 3354.
[13] M. Lazzeri, A. Vittadini and A. Selloni, Phys. Rev. B 63 (2001) 155409.
[14] A. Ghicov, J.M. Macak, H. Tsuchiya, J. Kunze, V. Haeublein L. Frey and P. Schmuki, Nano Lett. 6 (2006) 1080.
[15] S. Funk, B. Hokkanen, U. Burghaus, A. Ghicov and P. Schmuki, Nano Lett. xx (2007) xx.
[16] Z. Bing, S. Hermans and G.A. Somorjai, (eds.) Nanotechnology in Catalysis, Springer series: nanostructure science and technology (2004) ISBN 0-306-48323-8.
[17] K.R. Paserba and A.J. Gellman, Phys. Rev. Lett. 86 (2001) 4338.
[18] R.M. Slayton, C.M. Aubuchon, T.L. Camis, A.R. Noble N.J. Tro, J. Phys. Chem. 99 (1995) 2151.
[19] J. Wang, B. Hokkanen and U. Burghaus, Surf. Sci. 577 (2005) 158.
[20] M. Salmeron and G.A. Somorjai, J. Phys. Chem. 85 (1981) 3835.
[21] J.L. Brand, M.V. Arena, A.A. Deckert and S.M. George, J. Chem. Phys. 92 (1990) 5136.
[22] R.Z. Lei, A.J. Gellman and B.E. Koel, Surf. Sci. 554 (2004) 125.
[23] S. Funk, B. Hokkanen, J. Wang, U. Burghaus, G.H. Bozzolo and J.E. Garces, Surf. Sci. 600 (2006) 583.
[24] J. Ding, U. Burghaus and W.H. Weinberg, Surf. Sci. 446 (2000) 46.
[25] K.A. Fichthorn and R.A. Miron, Phys. Rev. Lett. 89 (2002) 196103.
[26] J. Wang, B. Hokkanen and U. Burghaus, Surf. Sci. 600 (2006) 4855.
[27] U. Burghaus, Surf. Rev. Lett. 8 (2001) 353.
[28] J. Wang and U. Burghaus, J. Chem.Phys. 122 (2005) 044705.
[29] C. Xu, B.E. Koel and M.T. Paffett, Langmuir 10 (1994) 166.
[30] S.L. Tait, Z. Dohnalek, C.T. Campbell and B.D. Kay, J. Chem. Phys. 122 (2005) 164707.
[31] S. Funk, T. Nurkic and U. Burghaus, Appl. Surf. Sci. 253 (2007) 4860.
[32] T. Kondo, D. Mori, R. Okada, M. Sasaki and S. Yamamoto, J. Chem. Phys. 123 (2005) 114712.
[33] Z.P. Hu, D.F. Ogletree, M.A. Van Hove and G.A. Somorjai, Surf. Sci. 180 (1987) 433.
[34] G.R. Darling and S. Holloway, Rep. Prog. Phys. 58 (1995) 1595.
[35] L. Vattuone, U. Valbusa and M. Rocca, Phys. Rev. Lett. 82 (1999) 4878.
[36] A. Gerbi, L. Savio, L. Vattuone, F. Pirani, D. Cappelletti M. Rocca, Angew. Chem. Int. Ed. 45 (2006) 6655.
[37] U. Burghaus, J. Stephan, J.M. Rogowska and L. Vattuone, A practical guide to Monte Carlo simulations and classical molecular dynamics simulations—An example book, NOVA science (2006) (New York, US), ISBN 1-59454-531-6.
[38] J. Stephan and U. Burghaus, Surf. Sci. 507–510 (2002) 736.